Available online at www.sciencedirect.com
SCIENCE DIRECT®
Journal of Nuclear Materials 337–339 (2005) 451–455
journal of nuclear materials
www.elsevier.com/locate/jnucmat

Measurement and modeling of hydrogen vibrational and rotational temperatures in weakly-ionized hydrogen discharges

E.M. Hollmann *, A.Yu. Pigarov, K. Taylor

Center for Energy Research, University of California at San Diego, La Jolla, CA 92093-0417, USA

Abstract

Neutral hydrogen molecule vibrational and rotational temperatures are measured using visible spectroscopy in two weakly-ionized, steady-state laboratory plasmas: a dc reflex-arc discharge and a rf etcher plasma. The rotational temperature in these experiments is found to be of order 5× less than the vibrational temperature, indicating that rotational internal energy should not be neglected if accurate neutral modeling of these plasmas is desired. A 0-D, steady-state model is developed which predicts measured ro-vibrational level populations within a factor of 10 or better and the overall vibrational and rotational temperatures within a factor of 2. In the plasma conditions studied here (electron density $10^8 < n_e < 10^{13}\,\mathrm{cm}^{-3}$, electron temperature $2 < T_e < 10\,\mathrm{eV}$), direct electron-impact excitation appears to be the dominant ro-vibrational heating mechanism, while wall collisions provide the dominant cooling mechanism.

PACS: 52.20.Hv; 52.25.Ya; 34.50.Ez
Keywords: Divertor modeling; Divertor neutrals; Hydrogen

1. Introduction

Vibrationally-excited neutral hydrogen molecules are known to play an important role in the chemistry of weakly-ionized hydrogen plasmas. For example, calculated rates for atom or proton exchange in ion-neutral collisions and atomic to molecular ion conversion depend strongly on the vibrational level of the interacting neutral hydrogen molecules [1]. In addition, it is likely that the rotational state of the H_2 molecules influences these reactions, since atomic/molecular interactions typically make use of the total energy available to the collision complex (translational, vibrational, and rotational) [2]. Comprehensive modeling of collision processes in cold, reactive hydrogen plasmas should, therefore, include both the rotational and the vibrational energy of the hydrogen molecules [3].

Here, the ability of presently available rate coefficient data to predict the ro-vibrational (rotational plus vibrational) distribution function of hydrogen molecules in typical laboratory plasma conditions is studied. Two different plasma devices are used: a reflex-arc discharge and a small helicon discharge. In both experiments, the ro-vibrational distribution function is modeled using an equilibrium, 0-D solution of the rate balance equations. Overall, it is found that the level densities of individual states is predicted within a factor of 10, while the shapes of the distribution functions (i.e., the vibrational

* Corresponding author.
E-mail address: ehollmann@ucsd.edu (E.M. Hollmann).

0022-3115/$ - see front matter © 2004 Elsevier B.V. All rights reserved.
doi:10.1016/j.jnucmat.2004.07.056

and rotational temperatures) are typically predicted within a factor of 2 or better.

2. Experimental setup

Fig. 1(a) shows a schematic of the dc reflex-arc discharge PISCES-A [4]. The measurements performed here are done in the target chamber region, which is typically isolated from the plasma source by a constricting baffle tube. Fig. 1(b) illustrates PISCES-A run without the baffle tube: in this case, the plasma volume is about twice as large. Typical experimental parameters for PISCES-A are: electron density $n_e \approx 10^{11}$–$10^{12}\,\mathrm{cm}^{-3}$ (10^{12}–$10^{13}\,\mathrm{cm}^{-3}$), electron temperature $T_e \approx 4$–$10\,\mathrm{eV}$, ion temperature $T_i \approx T_e$, neutral density $n_{H_2} \approx 2\times 10^{13}$–$5\times 10^{14}\,\mathrm{cm}^{-3}$ (2×10^{13}–$10^{14}\,\mathrm{cm}^{-3}$), and neutral translational temperature $T_{H_2} \approx 300$–$1000\,\mathrm{K}$ (1000–2500 K). Parentheses indicate ranges for baffle-free operation. Fig. 1(c) shows the rf helicon discharge, which is normally used for plasma etching studies [5]. The etcher discharge has typical parameters: $n_e \approx 10^8$–$10^{10}\,\mathrm{cm}^{-3}$, $T_e \approx 2\,\mathrm{eV}$, $T_i \approx 0.5\,\mathrm{eV}$, $n_{H_2} \approx 2\times 10^{14}$–$4\times 10^{14}\,\mathrm{cm}^{-3}$, and $T_{H_2} \approx 300\,\mathrm{K}$.

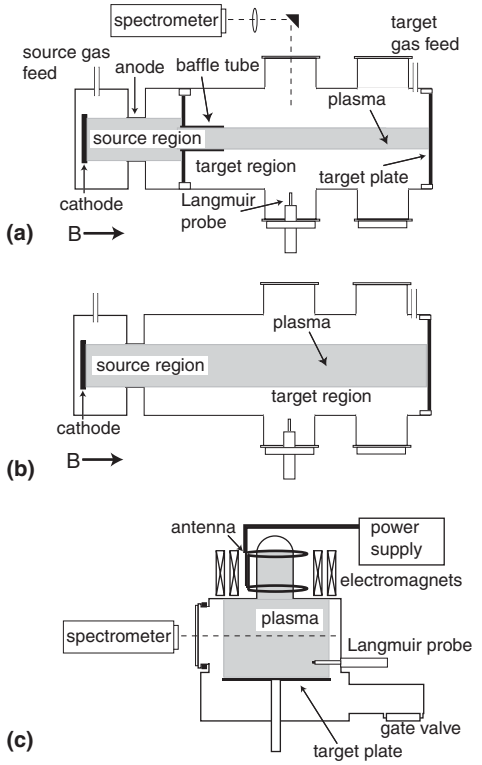

Fig. 1. Schematic of (a) PISCES-A reflex-arc discharge with constricting baffle tube, (b) PISCES-A without baffle tube and (c) rf etcher discharge.

In both PISCES-A and etcher plasmas, electron temperature and density are measured using Langmuir probe plunges. The hydrogen molecule translational temperature is obtained from the Doppler broadening of H_2 emission lines. The hydrogen molecule density is obtained from the hydrogen molecule temperature together with pressure gauge readings (atomic hydrogen pressure can be neglected here). The H_2 ro-vibrational distribution is obtained from the measured intensity of the diagonal (Q-branch) Fulcher ($d^3\Pi_u \rightarrow a^3\Sigma_g^+$) band. In the coronal limit, the electronic ground-state distribution N_{VJ} is determined by the matrix inversion:

$$I_{VJ} = g_J \delta_V \sum_{V'} Q_V^{V'} N_{VJ}, \tag{1}$$

where I_{VJ} is the measured line intensity with vibrational level V and rotational level J, g_J is the state degeneracy, δ_V is the line branching ratio, and $Q_V^{V'}$ is the vibrationally-resolved Frank–Condon matrix for $X'\Sigma_g \rightarrow d^3\Pi_u$ electron-impact excitation [6,7].

3. Ro-vibrational modeling

A 0-D model is developed which solves for the equilibrium population densities of the ro-vibrational levels of H_2. The collision processes included in the model are:

$$H_2(V,J) + e \rightarrow H_2(V',J') + e \quad \text{(eV)}$$

$$H_2(V,J) + e \rightarrow H_2^*(V'',J'') + e \rightarrow H_2(V',J') + e \quad \text{(eVx)}$$

$$H_2(V,J) + H^+ \rightarrow H_2(V',J') + H^+ \quad \text{(pV)}$$

$$H_2(V,J) + H^+ \rightarrow H_2^+(V',J') + H \quad \text{(CX)}$$

$$H_2(V,J) + e \rightarrow H_2^+(V',J') + 2e \quad \text{(eI)}$$

$$H_2(V,J) + e \rightarrow 2H + e \quad \text{(eD)}$$

$$H_2(V,J) + e \rightarrow H^- + H \quad \text{(DA)}$$

$$H_2(V,J) + H_2 \rightarrow H_2(V',J') + H_2 \quad \text{(H2V)}$$

$$H_2(V,J) + \text{wall} \rightarrow H_2(V',J') + \text{wall} \quad \text{(W)}$$

A summary of available vibrationally-resolved rate coefficient data for the electron and proton-impact processes (eV) through (DA) has been presented previously [8]. Amplitudes of the rotationally-resolved cross sections are estimated from the vibrationally-resolved ones by interpolation in the energy space E_{VJ}. For the cross sections (eV)–(eI), this assumes a smooth 2-D function $\sigma(V,J;V',J') = \sigma\ (E_{VJ};E_{V'J'})$; while for processes (eD) and (DA) a 1-D smooth function $\sigma(V,J) = \sigma(E_{VJ})$ is assumed. In all cases, the cross section vs. impact energy curve is shifted to the correct threshold energy before integrating over velocities to obtain the rate coefficient

$\langle\sigma v\rangle$. For electron and ion-impact processes resulting in a change in J, (eV)–(eI), the cross section for each possible final state J' is weighted by the relative statistical weight $g_{J'}/\sum_{J''} g_{J''}$, where the sum J'' is over all allowed final states. For direct electron-impact excitation (eV), the selection rule $\Delta J = 0, \pm 2$ is used, while for electron-impact excitation over excited electron states (eVx), a selection rule $\Delta J = 0, \pm 1$ is assumed. For proton-impact excitation (pV) and charge-exchange (CX), no selection rules are enforced, since these collisions are thought to access a broad distribution of J' values [9]. For simplicity, plasma ions are all assumed to be H^+ for the purposes of (pV) and (CX) rate calculations.

To estimate the ro-vibrational relaxation rate due to molecular impact (H2V), projectile molecules are assumed to in their statistical ground state (1/4 $H_2(0,0)$ and 3/4 $H_2(0,1)$). Calculated rate coefficients exist for these collisions for most target molecule initial and final states [10].

Wall relaxation (W) is the most uncertain rate in this model, with estimates for the probability of single-quantum vibrational relaxation ranging from 10^{-5} to 0.2 [11,12]. We assume a linear scaling in initial and final rotational angular momentum, as suggested in Ref. [13], giving transition probabilities:

$$P(V,J;V',J') = \begin{cases} \alpha(2J+1)(V+1)g_{J'}, & V - V' = \pm 1 \\ \beta(2J+1)g_{J'}, & V = V' \end{cases}. \quad (2)$$

Transitions which are not allowed energetically are assumed to have 0 probability, i.e., we require $E_{V'J'} - E_{VJ} \leqslant T_{H_2}$. Transition probabilities at high V, J are assumed to saturate at some maximum value P_{max}; this value is determined for each initial (V,J) state by enforcing conservation of probability, $\sum_{\substack{V'\neq V \\ J'\neq J}} P(V,J;V',J') \leqslant 1$. The coefficients α and β are left as free parameters.

To account for H_2^+ created by (CX) and (eI), we assume that H_2^+ is neutralized without changing its internal state as it collides with the wall, i.e., $H_2^+(V,J) \rightarrow H_2(V,J)$, which then relaxes according to the H_2-wall relaxation probability. To treat reactions (eD) and (DA), it is assumed that H and H^- which strike the wall are re-emitted as ground-state molecules.

From the pumping rate of the system, the inflow rate of fresh H_2 into the chamber can be estimated for steady-state operation. This inflow is assumed to be ground-state H_2. Outflow through the pumps is assumed to deplete all molecular states at the same rate.

To provide a qualitative overview of the relative importance of the various processes included in the model, the equilibrium loss rate of states $(V = 0,J)$ is plotted in Fig. 1 for a typical PISCES-A discharge. The loss rate is defined as $\nu_{loss}(V,J) \equiv \sum_{\substack{V'\neq V \\ J'\neq J}} \nu_{V,J}^{V',J'}$, where $\nu_{V,J}^{V',J'}$ is the single-direction rate of change from (V,J) into (V',J'). Outflow loss is labeled (S). It can be seen that cooling from wall collisions (W) is the largest single process for $J > 5$. This is balanced mostly by rotational excitation from direct electron impact (eV) and, at very high rotational levels $J > 20$, proton impact (pV). For low rotational quantum numbers $J < 4$, neutral collisions appear to be the dominant cooling term (Fig. 2).

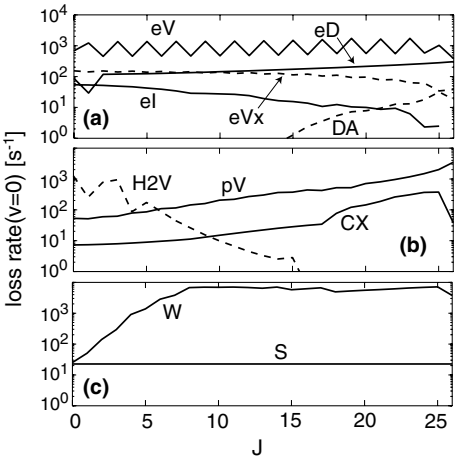

Fig. 2. Equilibrium loss rate out of states $(V = 0,J)$ for a typical PISCES-A plasma ($n_e = 10^{12}cm^{-3}$, $T_e = 6eV$, $P_{H_2} = 6mTorr$, $T_{H_2} = 500K$) due to (a) electron impact, (b) proton and neutral impact, and (c) outflow and wall collision processes.

4. Comparison with experiment

A given experimental condition is modeled by varying the model wall relaxation parameters α and β of Eq. (2) to minimize the error between the measured and modeled distribution functions, defined as $\sum_{V,J} |N_{V,J}^{(measured)} - N_{V,J}^{(model)}|$. The sum is taken over the limits $V = 0$–4 and $J = 1$–5; for higher V and J the coronal approximation, Eq. (1), is thought to begin loosing validity [14]. Sample measured and modeled distribution functions are shown in Figs. 3 and 4. In Fig. 3, the vibrational distributions are plotted for (a) $J = 1$, 3 and (b) $J = 2$, 4. The level density is shown divided by the statistical weight g_{VJ} and is plotted as a function of the state energy relative to the lowest energy state of each series, i.e., $\Delta E_{VJ} \equiv E_{VJ} - E_{0,J}$. Similarly, Fig. 4 shows the rotational distributions for (a) $V = 0$, 2 and (b) $V = 1$, 3. In this case, the state energy relative to the lowest energy state of each series becomes $\Delta E_{VJ} \equiv E_{VJ} - E_{V,0}$.

The dominant plasma parameter affecting the ro-vibrational distributions in these experiments is found to be electron density. A strong electron temperature dependence is not expected, due to the low threshold energy (~0.5 eV) for direct electron impact (eV) compared with the electron temperatures $2 < T_e < 10eV$ of these experiments.

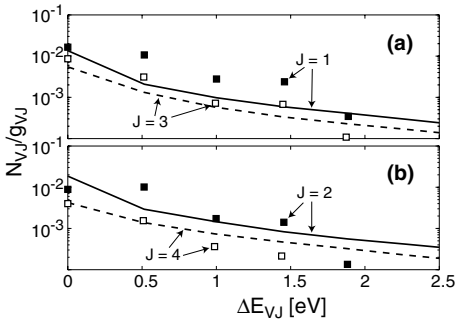

Fig. 3. Measured (points) and modeled (lines) vibrational distributions for (a) $J = 1$, 3 and (b) $J = 2$, 4.

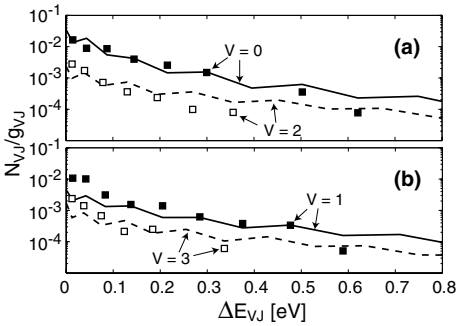

Fig. 4. Measured (points) and modeled (lines) rotational distributions for (a) $V = 1$, 3 and (b) $V = 2$, 4.

Fig. 5 shows the measured and modeled vibrational temperature as a function of electron density for the three different experimental configurations of Fig. 1. As was seen in Figs. 3 and 4, both experimental and modeled distributions tend to contain non-Boltzmann tails. Still, it is possible to study trends in the data by fitting the state densities for $V = 0$–4 and $J = 1$–5 to Boltzmann distributions with average vibrational and rotational temperatures T_{vib} and T_{rot}.

The diamonds in Fig. 5(a) show measurements taken in PISCES-A using helium plasmas with trace (<10%) quantities of hydrogen. These measurements do not deviate dramatically from the hydrogen plasmas, thus providing support for the prediction that electron impact, not ion impact, is the dominant ro-vibrational excitation mechanism.

The curves in Fig. 5 are calculated using measured electron temperatures and neutral densities, averaged over the entire data set. Because neutral kinetic temperature is not calculated in the present model, measured values of the neutral translational temperature T_{H_2} were fit to a smooth curve and input into the calculations. For PISCES-A, which has stainless steel walls, average values of the wall relaxation parameters were found to be

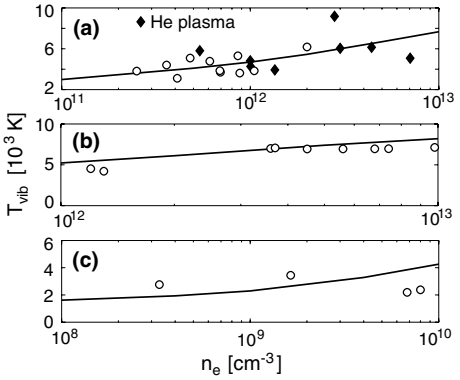

Fig. 5. Measured (points) and modeled (curves) vibrational temperatures T_{vib} as a function of electron density n_e for (a) PISCES-A with baffle tube, (b) PISCES-A with no baffle tube and (c) etcher plasma. Diamonds indicate helium discharges with trace H_2 injection.

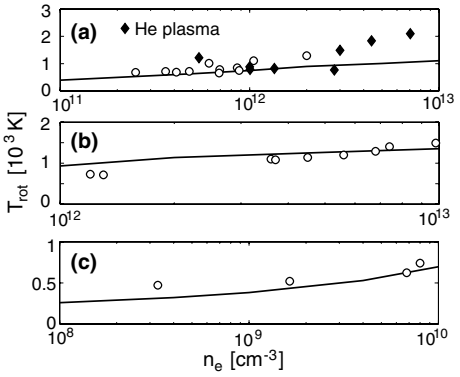

Fig. 6. Measured (points) and modeled (curves) rotational temperatures T_{rot} as a function of electron density n_e for (a) PISCES-A with baffle tube, (b) PISCES-A with no baffle tube and (c) etcher plasma.

$\alpha \approx 2.5 \times 10^{-4}$ and $\beta \approx 4.4 \times 10^{-5}$, while for the etcher experiment, which has aluminum walls, average values were $\alpha \approx 1.1 \times 10^{-5}$ and $\beta \approx 1.0 \times 10^{-5}$. Thus, hundreds of wall collisions are typically required for relaxation of a single ro-vibrational quantum.

Fig. 6 shows the measured and modeled rotational temperature as a function of electron density. As for the vibrational temperature, the model is found to match the data within a factor of 2, despite the wide range in neutral density and electron temperature in the measurements.

5. Discussion

The rotational temperature in these experiments is typically found to be only of order 5× less than the

vibrational temperature, demonstrating that rotational internal energy should not be neglected in a comprehensive treatment of weakly-ionized hydrogen plasmas. Interpolation in energy space starting with vibrationally-resolved rate coefficients is shown here to provide a reasonable starting point for rotationally-resolved modeling; however, accurate rotationally-resolved rate coefficient data are highly desirable for future work. We expect that modeling of the ro-vibrational distribution function will be especially crucial for understanding D^- sources [15], since dissociative attachment (DA) requires high ro-vibrational quantum levels and is, therefore, extremely sensitive to the shape of the non-Boltzmann tails seen in Figs. 3 and 4.

Acknowledgments

The authors wish to thank Dr S. Krasheninnikov, Dr R. Doerner, and Dr S. Brezinsek for helpful suggestions. The technical support of the PISCES-A staff is gratefully acknowledged. This work was supported by US DOE Grants No. DE-FG03-95ER54301 and DE-FG03-00ER54568.

References

[1] S.I. Krasheninnikov, A.Yu. Pigarov, D.A. Knoll, Phys. Plasmas 4 (1997) 59.
[2] R.D. Levine, Annu. Rev. Phys. Chem. 29 (1978) 59.
[3] S. Krasheninnikov, Phys. Scr. T 96 (2002) 7.
[4] D.M. Goebel, G. Campbell, R.W. Conn, J. Nucl. Mater. 121 (1984) 27.
[5] G.R. Tynan, A.D. Bailey III, G.A. Campbell, et al., J. Vac. Sci. Technol. A 15 (1997) 2885.
[6] B.P. Lavrov, A.S. Melnikov, M. Kaening, J. Roepcke, Phys. Rev. E 59 (1999) 3526.
[7] Z. Qing, D.K. Otorbaev, G.J.H. Brussaard, et al., J. Appl. Phys. 80 (1996) 1312.
[8] A.Yu. Pigarov, Phys. Scr. T 96 (2002) 16.
[9] B. Stewart, P.D. Magill, T.P. Scott, et al., Phys. Rev. Lett. 60 (1988) 282.
[10] D.R. Flower, E. Roueff, J. Phys. B 32 (1999) 3399.
[11] E.Ya. Kogan, V.N. Malnev, Ukr. Fiz. Zhur. 28 (1983) 374.
[12] A.M. Karo, J.R. Hiskes, R.J. Hardy, J. Vac. Sci. Technol. A 3 (1985) 1222.
[13] E.Ya. Kogan, V.N. Malnev, Sov. Phys. JETP 47 (1978) 276.
[14] B. Heger, U. Fantz, K. Behringer, J. Nucl. Mater. 290 (2001) 413.
[15] M. Bacal, G.W. Hamilton, Phys. Rev. Lett. 42 (1979) 1538.